Heliyon 10 (2024) e33585

Contents lists available at ScienceDirect

Heliyon

journal homepage: www.cell.com/heliyon

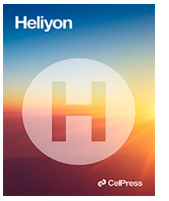

Research article

Lung decellularized matrix-derived 3D spheroids: Exploring silicosis through the impact of the Nrf2/Bax pathway on myofibroblast dynamics

Wenming Xue [a,b], Jiaxin Wang [a,b], Yao Hou [a,b], Di Wu [a,b], Hongwei Wang [a,b], Qiyue Jia [a,b], Qiyue Jiang [a,b], Yan Wang [a,b], Chenzhao Song [c], Yifei Wang [d], Zhonghui Zhu [a,b,**], Lin Tian [a,b,*]

[a] Department of Occupational and Environmental Health, School of Public Health, Capital Medical University, Beijing, 100069, China
[b] Beijing Key Laboratory of Environmental Toxicology, Capital Medical University, Beijing, 100069, China
[c] Department of Pathology, Beijing Youan Hospital, Capital Medical University, Beijing, 100069, China
[d] Experimental Teaching Center of Public Heatlh and Preventive Medicine, School of Public Health, Capital Medical University, China

ARTICLE INFO

Keywords:
Silica
3D culture
Myofibroblasts
Nrf2
Apoptosis
Fibrosis

ABSTRACT

Silicosis is an occupational respiratory disease caused by long-term inhalation of high concentrations of free silica particles. Studies suggest that oxidative stress is a crucial initiator of silicosis fibrosis, and previous studies have linked the antioxidative stress transcription factor known as Nrf2 to fibrosis antagonism. Myofibroblasts play a pivotal role in tissue damage repair due to oxidative stress. Unlike physiological repair, myofibroblasts in fibrosis exhibit an apoptosis-resistant phenotype, continuously synthesising and secreting significant amounts of collagen and other extracellular matrices, which could be a direct cause of silicosis fibrosis. However, the relationship and mechanism of action between oxidative stress and myofibroblast apoptosis resistance remain unclear. In this study, a new 3D cell culture model using mice lung decellularised matrix particles and fibroblasts was developed, simulating the changes in myofibroblasts during the development of silicotic nodules. Western Blot results indicate that silica stimulation leads to increased collagen deposition and decreased apoptosis-related protein Bax and oxidative stress-related protein Nrf2 in the 3D spheroid model. Immunofluorescence experiments reveal co-localisation in their expression. In Nrf2 overexpressing spheroids, Bax exhibits significant upregulation. In the Nrf2 knockout spheroids, Bax is also significantly downregulated; after intervention with Bax inhibitors, a significant downregulation of Bax-induced apoptosis was also detected in the Nrf2-overexpressed spheroids. In contrast, Bax-induced apoptosis showed a significant upregulation trend in Nrf2-overexpressed spheroids after intervention with Bax agonists. The results demonstrate that the spheroid model can mimic the development process of silicotic nodules, and silica stimulation leads to an apoptosis-resistant phenotype in myofibroblasts in the model, acting through the Nrf2/Bax pathway. This research establishes a new methodology for silicosis study, identifies therapeutic targets for silicosis, and opens new avenues for studying the mechanisms of silicosis fibrosis.

* Corresponding author. Department of Occupational and Environmental Health, School of Public Health, Capital Medical University, No. 10, Xitoutiao Youanmen Street, Beijing, 100069, China.

** Corresponding author. Department of Occupational and Environmental Health, School of Public Health, Capital Medical University, No. 10, Xitoutiao Youanmen Street, Beijing, 100069, China.

E-mail addresses: zhuzhonghui@163.com (Z. Zhu), tian_lin@163.com (L. Tian).

https://doi.org/10.1016/j.heliyon.2024.e33585
Received 21 March 2024; Received in revised form 23 June 2024; Accepted 24 June 2024
Available online 24 June 2024

1. Introduction

With the rapid economic growth and increasing industrial demands, many workers are exposed to high concentrations of silica particles. Long-term inhalation of high concentrations of free silica can lead to silicosis. This condition, marked by silica nodules and widespread lung fibrosis, presents significant health hazards [1–3]. The causative agent of silicosis is well-established, but its pathogenic mechanisms remain elusive. A more profound understanding of how silica contributes to lung fibrosis is essential for devising effective countermeasures and treatments for this disease.

Myofibroblasts are central to silicosis fibrosis, primarily due to their excessive collagen secretion leading to lung fibrosis. Hence, myofibroblast research is pivotal in understanding silicosis fibrosis. Traditionally, fibroblasts have been studied in two-dimensional cultures, which lack the extracellular matrix, limiting their ability to mimic in-vivo cell environments [4–6]. The advancement in three-dimensional (3D) cell culture technologies has enhanced cell model development. Notably, Shilpaam [7] established a robust lung tuberculosis model by co-culturing macrophages and fibroblasts, delineating the biological features of 3D tuberculosis spheroids. While various 3D models have been developed using diverse cultivation techniques, models explicitly related to silicosis are limited. In this study, the mouse lung decellularised matrix (LDM) and fibroblasts were used to create a self-assembling 3D lung spheroid model. This model enables a deeper exploration of fibroblast changes in silicosis progression.

Research has revealed that inhaled silica can stimulate the body to produce numerous inflammatory factors and reactive oxygen species (ROS), placing the body in an oxidative stress environment that contributes to the onset of fibrosis. Consequently, oxidative stress is a significant initiator of silicosis [8,9]. Nuclear factor erythroid 2-related factor 2 (Nrf2) plays a crucial role in cellular defences against oxidative stress and ROS. During oxidative stress, Nrf2 can migrate to the cell nucleus to exert antioxidant effects [10,11]. Studies, including those by Louise et al. have shown that oxidative stress imbalance involving Nrf2 could be a driving factor in promoting lung fibrosis [12]. Previous research reported that activating Nrf2 helps combat fibrosis in mice lungs, making Nrf2 a vital therapeutic target in lung fibrosis [13]. It is well-known that fibroblasts play an essential role in tissue repair caused by oxidative stress. Under normal conditions, fibroblasts can undergo programmed death following tissue repair processes [14,15]. However, research suggests that in idiopathic pulmonary fibrosis, myofibroblasts exhibit increased apoptosis resistance, termed the ‘apoptosis paradox’ [16]. The presence of apoptosis-resistant myofibroblasts leads to substantial collagen deposition, an essential aspect of pulmonary fibrosis [17,18]. Thus, studying oxidative stress and the apoptosis resistance mechanism of myofibroblasts could be beneficial in combating silicosis fibrosis. Currently, extensive research exists on the relationship between oxidative stress and apoptosis, but there is limited study on any correlation concerning silicosis development. In the current study, there is a regulatory relationship between oxidative stress, represented by Nrf2, and apoptosis resistance in myofibroblasts during fibrosis. This interaction seems to operate through the Nrf2/Bax pathway.

In conclusion, this research establishes a novel 3D pulmonary spheroid model to simulate the development and onset of silicosis. A thorough examination was conducted on the apoptosis resistance characteristics of myofibroblasts, clarifying the temporal relationship between oxidative stress and apoptosis, and unraveling potential regulatory pathways controlling myofibroblast apoptosis. These findings pave the way for new approaches in combating silicosis fibrosis and facilitate the identification of effective therapeutic drugs.

2. Methods

2.1. Preparation of lung decellularized matrix

Three-month-old C57BL/6 J mice were provided by SPF Biotechnology Co. Ltd. (Beijing, China) and were raised under specific pathogen-free conditions. Mice were injected with sodium heparin solution (Solarbio, P10200, China) before sacrifice. Thoracic dissection was then performed. After opening the chest, the lungs and the heart were found, using a perfusion needle about 2 mm into the pulmonary artery above the left auricle, clamped and fixed and then injected with sodium heparin (i.p.) solution, after observing that the color of the lung tissue changed to white, the intact free heart and lungs were connected to the Langendorff extracorporeal perfusion system (ZHONGSHI DICHUANG TECHNOLOGY DEVELOPMENT, ZS-LF, China). The heparinized PBS solution was flushed at a constant flow rate and temperature (0.5 mL/min, 25 °C) for 15 min, then injected the following solutions of the corresponding duration: 1 % sodium deoxycholate for 120 min (Sigma-Aldrich, 302-95-4, USA), 1 % Triton X-100 for 10 min (BEIJING DINGGUO CHANGSHENG BIOTECHNOLOGY CO.LTD, DH351-4, China), DNase I rinse solution for 60 min (Solarbio, D8071, China) and antibiotic rinse solution for 60 min (Solarbio, S8252, China). After all of the above solutions were perfused, perfusion was stopped to obtain whole lung decellularized matrix scaffolds, and the decellularized matrix used for the preparation of pathology was put into 4 % paraformaldehyde solution and stored in a refrigerator at 4 °C; the decellularized matrix particles used for the preparation of decellularized matrix particles were drained and put into 15 mL centrifugal tubes, and stored at −80 °C. After accumulating a certain number of decellularized lungs, the decellularized lungs were ground at high speed inside the Liquid Nitrogen-filled Freezer/Mill cryogenic pulverizer, with the parameters set as Precool 5 min, Cool time 1 min, run time 2 min, cycle course: 3, rate 15, and the decellularized lung matrix powder was obtained after net sufficient grinding, and the powder was collected and stored in liquid nitrogen.

2.2. Preparation of silica-stimulated macrophage supernatant

Inoculated 2×10^7 macrophages (RAW264.8) into a new 9 mm culture dish (Thermo, 150464, USA). After 24 h, discarded the

culture medium, macrophages were stimulated by adding serum-free DMEM (Corning Incorporated, USA, 10-013-CV) containing 50 μg/mL silica to the petri dishes. Then, after 24 h, the supernatant was passed through a filter membrane, and the clarified supernatant was stored at −80 °C for future use.

2.3. Establishment of 3D cell culture model

NIH/3T3 cells were cultured in DMEM containing 10 % newborn calf serum (gibco, 16010159, USA) and 1 % penicillin–streptomycin (KeyGEN Bio TECH, KGY0012, China). When cells were cultured to the experimental generation, collected the cells suspensions. Complete medium, cells suspension, and decellularized lung matrix powder were added into the wells of an ultra-low adsorption plate (STEMCELL Technologies, 34415, Canada) in turn. Each well contained 3×10^6 cells to construct the 3D spheroid model. The cultures were incubated at 37 °C in a 5 % CO_2 constant-temperature incubator. After 24 h, 1 mL of complete medium containing 20 % newborn calf serum was replaced, and after another 24 h, when the morphology of the spheroids in the well plates became homogeneous and the borders were well defined, the spheroids were transferred out into flat-bottomed 24-well ultra-low adsorbent plates (LABSELECT, 11318, China) and for intervention. Silica-stimulated macrophage supernatant (concentration of silica was 50 μg/mL) was added to the experimental group. Macrophage supernatant without silica stimulation was added to the control group. 1/3 of the culture solution was renewed daily. The 3D models were assayed after 1, 7, and 14 days. Afterwards we refer to silica-free macrophage supernatant as conditioned medium (simply known as CM) and to silica-stimulated macrophage supernatant as silica-containing conditioned medium (simply known as CM-Silica).

2.4. Scanning electron microscopy

The spheroids were removed from the plates and fixed using 2.5 % glutaraldehyde (Solarbio, #P1126, China) for 2 h to stop cell activity. Upon completion, they were washed with PB buffer then dehydrated with gradient ethanol (50 %, 70 %, 80 %, 90 %) for 10 min each time and anhydrous ethanol for 2 min. After dehydration was completed, the samples were transferred to mica sheets and the spheroids, particles of decellularized matrix dissolved using purified water, and lung decellularized matrix were dried in an oven, followed by a week of drying in a desiccant. After complete drying, the above samples were coated (7 nm) on a conductive tape of the sample stage and photographed (S-4800, Hitachi Limited, Japan).

2.5. Histological staining

Samples were prepared by paraffin sectioning. The cell surface morphology of the sections was observed by hematoxylin-eosin (HE) and Masson (MS) staining.

HE staining. The paraffin sections were deparaffinized in xylene. After dewaxing, they were rehydrated in an ethanol gradient (100 %, 95 %, 85 %, 75 %). After rehydration, the sections were rinsed in distilled water. Then dyed with hematoxylin solution and washed with distilled water to remove excess dye. The paraffin sections were then incubated in differentiation solution and then washed with water. The sections were then placed in eosin dye, followed by washing with distilled water. For rapid dehydration, the samples were soaked 75 %, 85 %, 95 %, and 100 % ethanol, followed by a 1-min soak in another 100 % ethanol. To improve transparency, the sections were soaked in xylene. Finally, the sections were sealed with neutral gum and observed under the microscope.

MS staining. The paraffin sections were deparaffinized in xylene and then in anhydrous ethanol. They were then successively incubated in 95 %, 90 %, 80 %, and 70 % ethanol. After washing with distilled water, the paraffin sections were placed in MS complex dyeing solution. After dyeing, the paraffin sections were washed with 1 % glacial acetic acid. The slices were then dehydrated by successively incubating twice in 95 % alcohol, twice in anhydrous ethanol, and twice in xylene. Finally, the sections were sealed with neutral gum and observed under the microscope.

2.6. Antibodies and reagents

Samples of spheroids and samples of decellularized lungs/normal mice lungs were subjected to SDS-PAGE on a 10 % gel. Antibodies used were Collagen I (1:500, Santa Cruz, sc293182, USA), GAPDH (1:1000, Cell Signaling Technonogy, 2118s, USA), Laminin γ-3 (1:1000, Immunoway, YT253, USA), Collagen III (1:1000, Immunoway, YM3123, USA), Collagen IV (1:1000, abcam, ab236640, USA), α-SMA (1:500, ab7817, abcam, USA), Nrf2 (1:1000, 16396-1-AP, Proteintech, USA), Bcl-2 (1:1000, Immunoway, YT0407, USA), Caspase-3 (1:1000, abcam, ab179517, USA), Bax (1:1000, abcam, ab32503,USA), Bak (1:1000, Immunoway, YT0049, USA). ECL assay reagent (Absin, P10200, China) was used to detect the signal, and the signal was detected by the Tanon- 5200 system (Beijing Yuanpinghao Biotechnology Co, Ltd., Tanon- 5200 system, China).

2.7. Immunofluorescence

Immunofluorescence double staining assay using mouse and rabbit double standard three-color fluorescence detection kit (Immunoway, RS0036, USA). The paraffin sections of spheroids were deparaffinized according to the instructions, after closure, incubated with Nrf2 primary antibody (1:200, Proteintech, 16396-1-AP, USA) dropwise for 1 h at 37 °C, washed with PBS and then incubated with secondary antibody and fluorescent dye D594 dropwise successively for 30 min and 10 min at room temperature. After that, the above steps were repeated, and then Bax primary antibody (1:200, abcam, ab32503, USA) was added dropwise after PBS

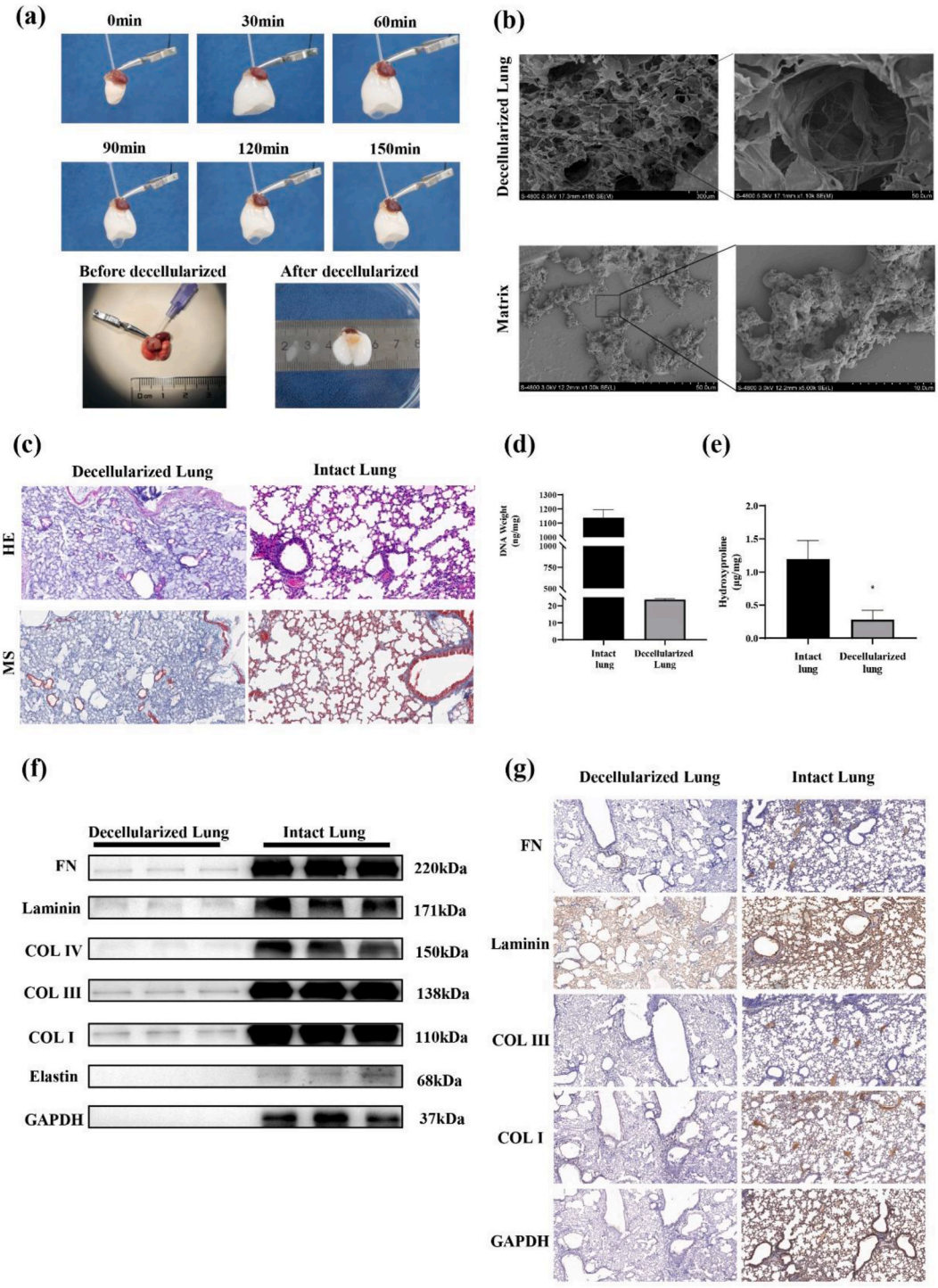

Fig. 1. (a) Schematic representation of mouse lung from anatomical isolation to completion of decellularisation. (b) Scanning electron micrograph of decellularised matrix of mouse lung (top) and scanning electron micrograph of decellularised matrix granules of mouse lung (bottom). (c) Histopathologic staining diagrams of normal mouse lung and mouse lung after decellularisation treatment. (d) Picogreen method for detecting DNA dry weight in normal mouse lungs and decellularised mouse lung tissues. (e) Hydroxyproline assay results in lungs of decellularised mice and normal mice. *: $p < 0.05$. All data are shown as means ± SD. (f) Western Blot analysis and immunohistochemical analysis of normal mice lungs and mice lungs after decellularisation treatment. (g) Immunohistochemical detection of related proteins in normal mouse lungs and decellularised mouse lungs.

washing and incubated at room temperature with secondary antibody and fluorescent dye D-488 successively. After antigen repair, the slices were sealed with DAPI-containing sealer. The slices were observed and photographed under a Nikon confocal microscope (ECLIPSE Ti2, Nikon, Japan).

2.8. Establishment of cell lines

Lentiviral vectors overexpressing Nrf2 and silencing Nrf2 were obtained from Genechem Corporation (Genechem Corporation, China). Transfection was performed in NIH/3T3 cells according to the manufacturer's instructions. Nrf2 overexpressing NIH/3T3 cell lines were established using lentiviral transfection technique, and successful transfected NIH/3T3 cells were screened using puromycin; Nrf2-silenced NIH/3T3 cell lines were constructed using CRISPR/Cas9 gene editing technique, and successful transfected NIH/3T3 cells were screened using G418 and puromycin.

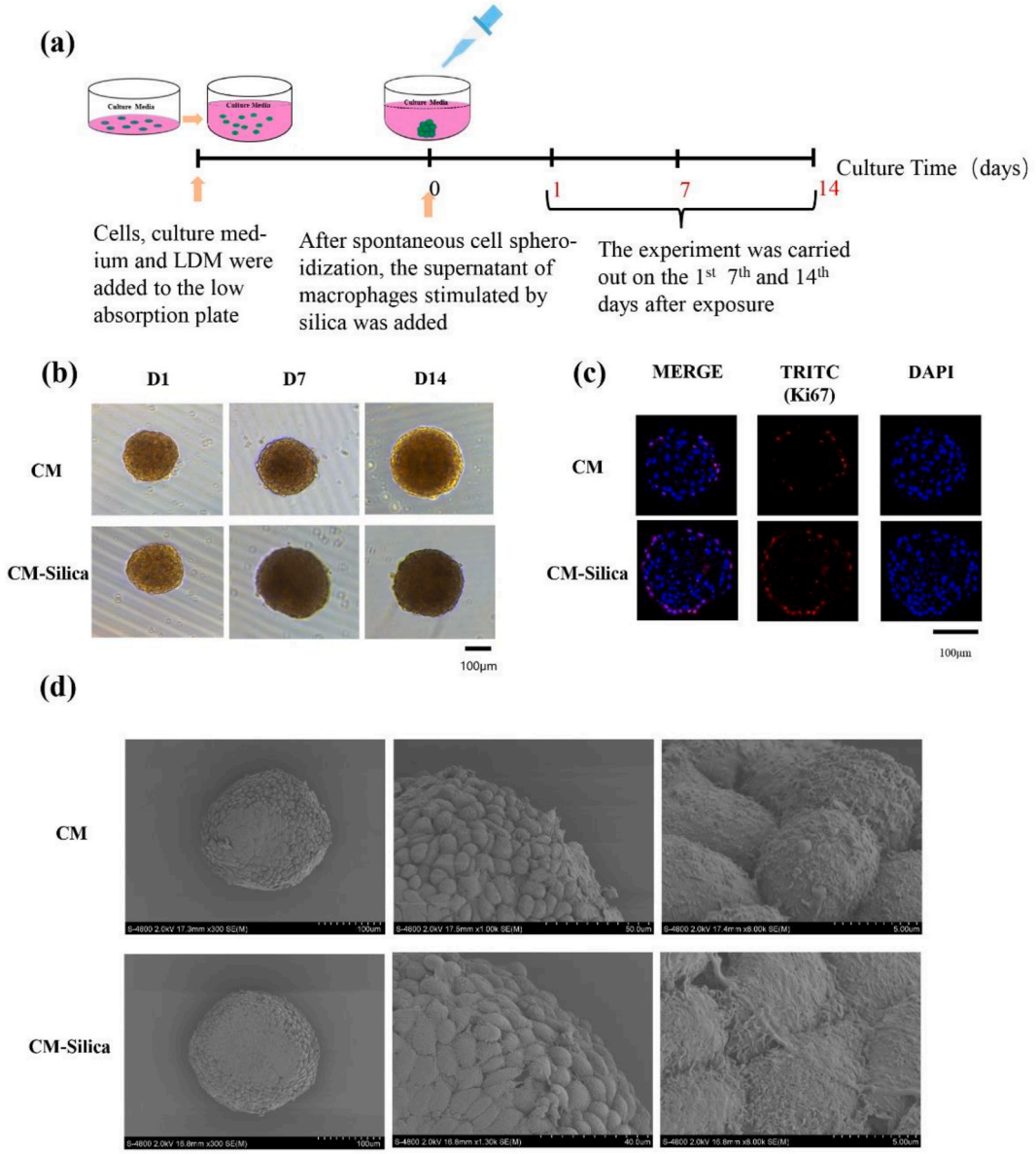

Fig. 2. (a) Modeling process of 3D spheroids model. (b) Scanning electron micrographs of 3D spheroids models after 1, 7 and 14 days of intervention using macrophage supernatant with/without silica stimulation. (c) Ki67 protein expression in 3D spheroids models after 1, 7 and 14 days of intervention using macrophage supernatant with/without silica stimulation. (d) Scanning electron micrographs of 3D spheroids models after intervention using macrophage supernatants with/without silica stimulation.

2.9. Statistical analysis

All statistical analyses were performed using the SPSS software, version 20.0 (SPSS, Chicago, USA). The independent samples T test was applied to compare the two group, and one-way analysis of variance (ANOVA) was applied to compare the mean values among multiple groups. Data were presented as the mean ± SD. The value of $p < 0.05$ was considered statistically significant.

3. Result

3.1. Acquisition and detection of lung decellularised stroma

The intact decellularised stroma of mice lungs were developed by using pulmonary artery perfusion (Fig. 1(a)). After the decellularisation treatment, mice lungs appeared white and translucent, with intact lobe structures and relatively clear structures such as veins and bronchi. Removal of cellular components was necessary to obtain the decellularised matrix of the lungs. Scanning electron microscopy, histopathological staining, and determination of DNA content in normal mouse lungs and decellularised lungs were used to determine the effectiveness of decellularisation therapy. The electron microscopy results showed (Fig. 1(b)) that the decellularized mice lungs are porous structures with collagen fibres showing a tangled stripe-like distribution, and no cell morphology or structure is observed. HE staining results show (Fig. 1(c)) that the normal mice lungs are structurally intact, with the alveolar epithelial cells neatly arranged and tightly packed. After decellularisation, the structure of the lung tissues is still intact, but the hematoxylin-stained nuclei basically disappear. The results of MS staining show that the blue collagen structure of the lungs of the decellularised mice lungs is more apparent. The DNA content test results showed that (Fig. 1(d)) the dry weight of DNA in normal mouse lung tissue is 1138.34 ± 56.44 ng/mg, while in decellularised mouse lung tissue, the dry weight of DNA is 23.70 ± 0.45 ng/mg. The DNA content in the lung tissue of decellularised mice is less than the standard 50 ng/mg, indicating that the decellularisation treatment method is effective and removes the vast majority of nucleic acids from the tissue.

The results of hydroxyproline detection show (Fig. 1(e)) that after decellularisation treatment, the collagen fibre content in the lungs of mice is significantly reduced, indicating that decellularisation treatment can cause a significant loss of collagen in the lung tissue of mice. To investigate the components of a decellularised matrix, Western Blot and immunohistochemical analysis are used to detect normal mouse lungs and decellularised mouse lungs. In Fig. 1(f and g), cytoplasmic protein representative GAPDH is significantly reduced in the decellularised lungs, implying the effectiveness of the decellularisation process.Additionally the main retained components present are matrix proteins such as COL I/III, fibronectin and Laminin. The significantly reduced collagen content is consistent with the hydroxyproline detection data.

The above results indicate that an intact decellularised matrix is present, and the decellularisation treatment resulted in the fundamental shedding of cells under the basement membrane and took away some of the collagens in the basement membrane, such as fibronectin and laminin. The main components of the decellularised matrix are still COL I and III, fibronectin, and Laminin.

3.2. 3D spheroids modeling and morphology observation

NIH/3T3 cells, in combination with lung decellularised matrix particles, were used to construct self-assembled 3D lung spheroids models, and the process is shown in Fig. 2(a) (detailed in the Supplementary Material). After the 3D model was stabilised into a spherical shape, the 3D spherical model was stimulated using a silica-stimulated macrophage supernatant to mimic the stimulation effect of silica upon entry into the organism, with reference to the intervention method previously studied in this study [13]. The spheroids model was analyzed under the light microscope at 1, 7, and 14 days of intervention (Fig. 2(b)), with the diameter of the spheroids showing an increasing trend with the prolongation of incubation time, suggesting that the cells in the spheroids are in a good state of growth. Immunofluorescence experiments were performed for Ki67 protein on the spheroids model after seven days of intervention (Fig. 2(c)), and the results showed that the peripheral cells of the model are in a stable proliferative state, suggesting that the model construction is successful. Scanning electron microscopy was used to observe the 3D spheroids seven days after the intervention of silica-stimulated macrophage supernatant. The results showed (Fig. 2(d)) that the spheroids yield cells that are tightly packed together, and the surfaces of the spheroids cells showed more striated collagen fibre bundles structures after administration of silica-stimulated macrophage supernatant compared to the CM group.

The results suggest that the spheroids model was constructed successfully and that 3D spheroids may exhibit a trend toward increased collagen secretion and deposition after the stimulation with silica-stimulated macrophage supernatant was given.

3.3. Silica stimulation promotes collagen deposition in 3D spheroids

In order to clarify the cell changes inside the 3D spheroids after silica stimulation and collagen deposition, they were examined from two perspectives: pathological staining and quantification using Western Blot. The HE results showed that with the intervention of silica-stimulated macrophage supernatants, the number of nuclei is significantly reduced, mainly in the form of a significant reduction of spherical center cells in the three-dimensional structure (using the number of cell Nuclei Per Unit Area as a quantitative index for HE staining of the spheroids, calculation: the ratio of the number of nuclei to the area of the cell spheroid, Fig. 3(a)). Additionally, the number of Nuclei Per Unit Area decreases with the extension of incubation time, and the “polarisation phenomenon” of unilateral aggregation of nuclei appears. The results of Masson staining showed that the Collagen Volume Fraction in the CM-silica group is significantly higher than that in the CM group, and tends to increase with increasing incubation time (using the Collagen

Volume Fraction as a quantitative indicator of Matson staining for the model, calculation: ratio of blue collagen area to cell spheroid area, Fig. 3(c)). The collagen volume fraction in the CM-silica group is significantly higher than that in the CM group and increased with increasing incubation times. The deposited collagen gradually aggregates to the spheroid centre, especially on the 14th day. The collagen deposits in the spheroid in an apparent concentric arrangement, similar to the pathological structure of the silica nodules in vivo.

The relative expression levels of proteins in CM and CM-silica spheroids were analyzed. The results show that the levels of fibrosis-associated proteins COL I, COL III, and α-SMA are increased in the CM-silica group after 1, 7, and 14 days of silica stimulation ($p < 0.05$). Notably, short-term silica stimulation (1 day) results in a more pronounced up-regulation of α-SMA, an indicator of fibroblast activation, in the up-regulation in the CM-silica group as compared to the long-term (7 and 14 days), and the long-term stimulation induces more pronounced collagen deposition. The, experimental results infer that silica stimulates the proliferation and differentiation of fibroblasts into myofibroblasts and the production of collagen deposition in spheroids, promoting spheroid's fibroblast-like changes.

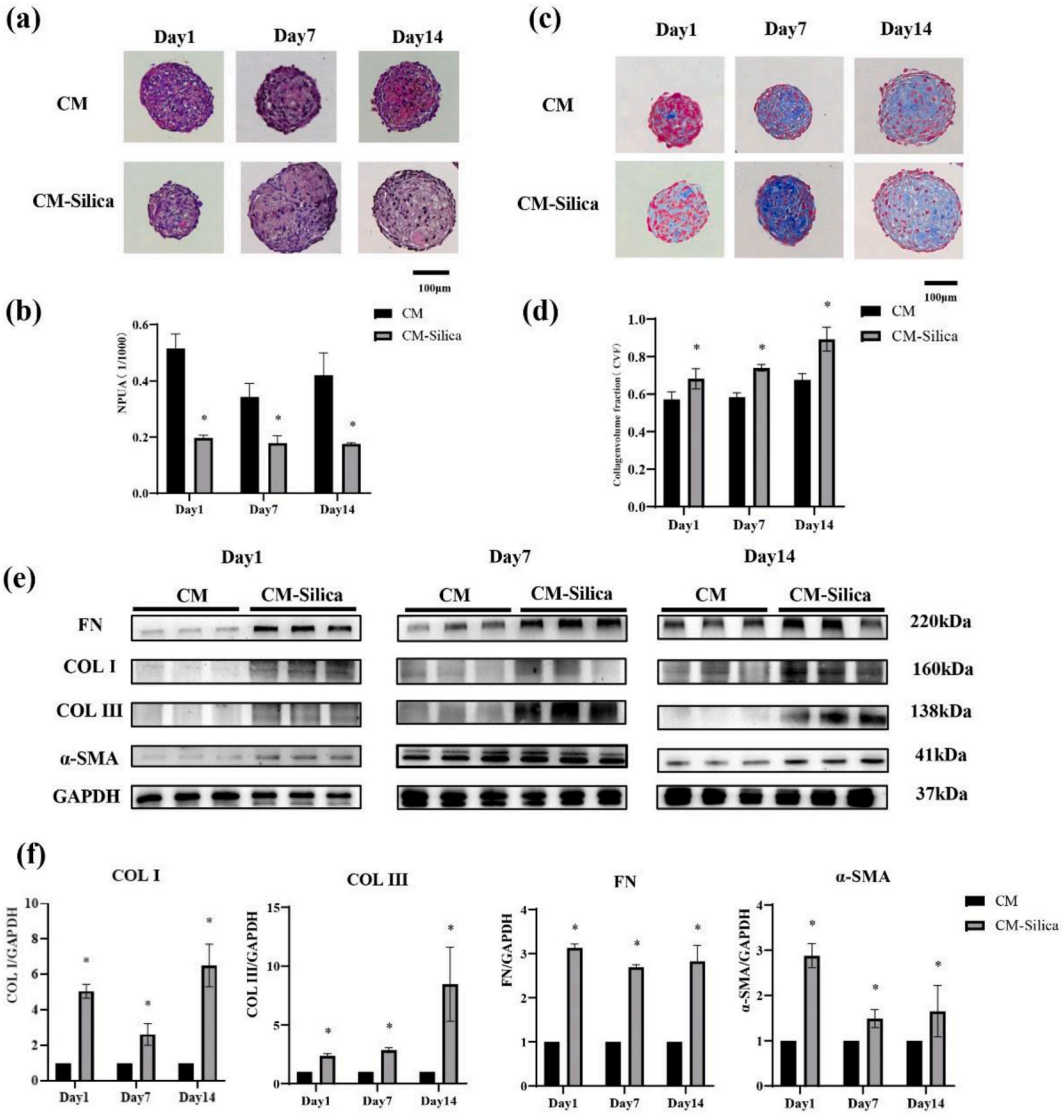

Fig. 3. (a) HE staining of 3D spheroids models using macrophage supernatants with/without silica stimulation for stimulation 1, 7, and 14 days. (b) The Number of Nuclei Per Unit Area (NPUA) was used as a quantitative index of HE staining, and the results were analyzed statistically. (c) Masson staining of 3D spheroid models using macrophage supernatants with/without silica stimulation for stimulation 1, 7, and 14 days. (d) Statistical analysis of Collagen Volume Fraction (CVF) as a quantitative index of Masson staining. (e) Western blotting analysis of fibrosis-related indexes: COL I, COL III, α-SMA in 3D spheroids models stimulated using macrophage supernatant with/without silica stimulation for 1, 7, and 14 days. (f) Results of statistical analysis of grey values. n = 3 compared to control, *: $p < 0.05$. All data are shown as means ± SD.

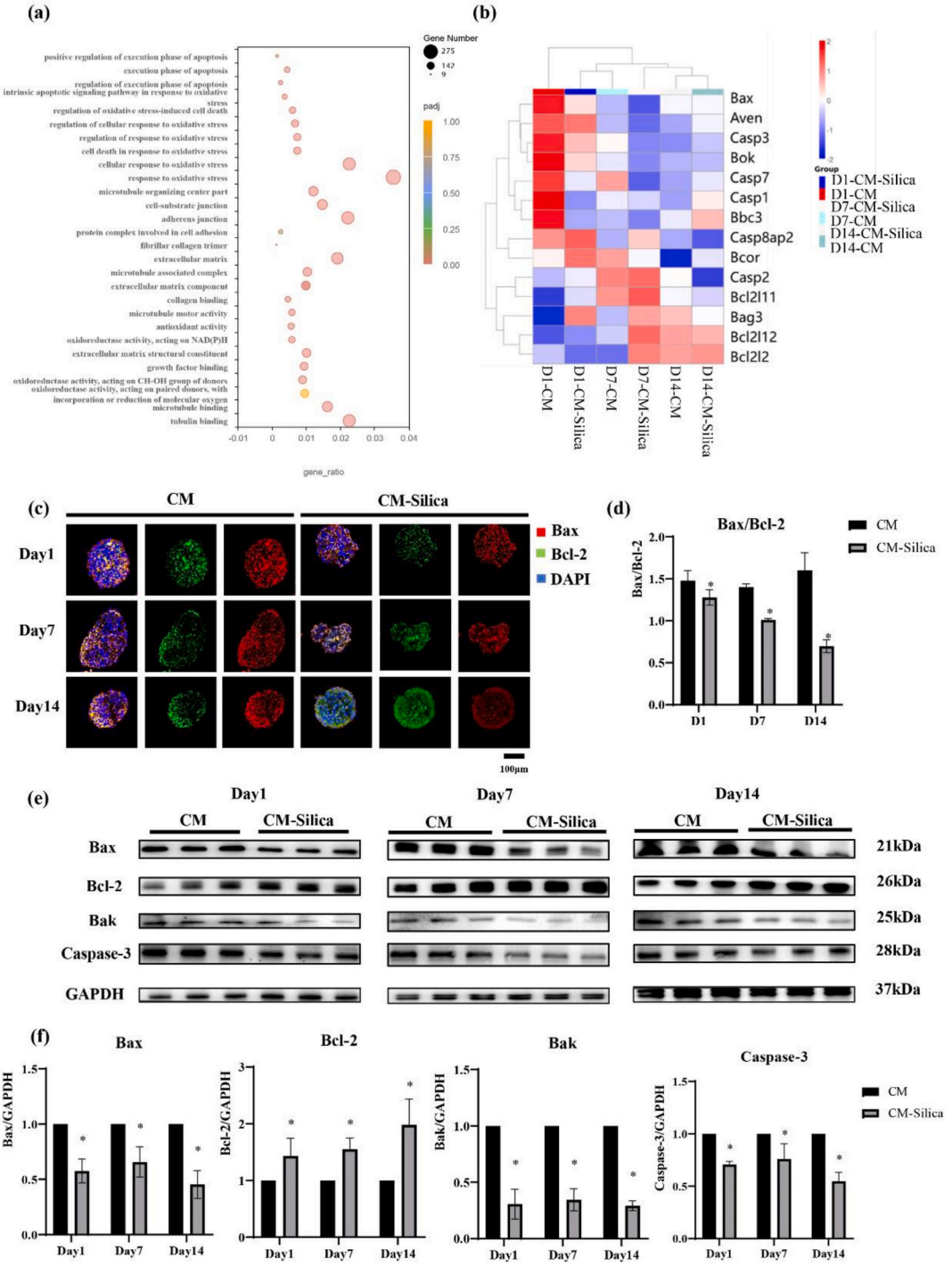

Fig. 4. (a) GO enrichment results of differential genes in the 3D model after stimulating spheroids with/without silica-stimulated macrophage supernatant for seven days. (b) Heatmap of apoptosis-related gene changes from RNA-seq analysis. (c) Immunofluorescence double-staining results of Bax (Red) and Bcl-2 (Green) proteins in spheroids were plotted. (d) Statistics of fluorescence intensity analysis results of Bax and Bcl-2, n = 3, *: $p < 0.05$ compared with NC, DAPI (Blue). (e) Western blotting analysis results of spheroids apoptosis-related indicators Bax, Bcl-2, Bak, and Caspase-3 after stimulation of spheroids with/without silica-stimulated macrophage supernatant for 1, 7, and 14 days. (f) Results of statistical analysis of grey values, n = 3, *: $p < 0.05$ compared with NC. All data are expressed as mean ± SD. (For interpretation of the references to color in this figure legend, the reader is referred to the Web version of this article.)

3.4. Silica leads to apoptosis resistance in 3D spheroids

The relevant genes within silica-stimulated spheroids on days 1, 7, and 14 were analyzed using RNA sequencing and analyzed Gene Ontology (GO) enrichment of differential genes in the CM-Silica group after 1 and 14 days of intervention (Fig. 4(a)). Biological processes such as oxidative stress, apoptosis and ECM remodeling in spheroids are significantly altered with the extension of culture time, as evidenced by the increase in response to oxidative stress, oxidative stress acting on NADPH, the increase in the cellular response to apoptosis, the increase in synthesis of extracellular matrix, and up-regulation of the level of cell-to-cell adhesion. The heatmaps of the relevant genes after 1, 7 and 14 days of intervention show apoptosis-related genes, such as Bax and Casp3, are down-regulated and the anti-apoptosis gene Bcl-2 displays an up-regulation trend in the silica groups incubated for 1, 7 and 14 days, compared with their respective controls. The down-regulation trend of the apoptosis-related genes correlates as a down-regulation with increasing incubation time. In contrast, the up-regulation trend of the anti-apoptosis genes demonstrated an up-regulation with the incubation time as well (Fig. 4(b)). The sequencing results were then validated at the protein level. Immunofluorescence staining for Bcl-2 (Green) and Bax (Red) proteins is performed on spheroids from intervention days 1, 7 and 14 (Fig. 4(c)). The results show that compared with the CM group, after apoptosis-related protein Bax is down-regulated in the CM-Silica group and tended to be down-regulated with the prolongation of the incubation time. In contrast, the anti-apoptotic protein Bcl-2 shows up-regulation and is gradually up-regulated with increasing incubation times. It can be found in the spheroids space structure that both exhibit high expression in the cytoplasm and almost no expression in the nucleus. The fluorescence intensity of each group of spheroids (Fig. 4(d)) is assessed, with the expression of apoptosis-related proteins Bax and Bcl-2 in the spheroids displaying apoptosis-resistant trends (the statistical index is the fluorescence intensity of Bax/the fluorescence intensity of Bcl-2, and a decrease in the index indicates that Bax is decreased or Bcl-2 is elevated, both of which represent apoptosis resistance). Afterwards, Western blotting experiments on spheroids from each group (Fig. 4(e)) showed that compared with the CM group, the spheroids apoptosis-related proteins Caspase-3, Bax, and Bak are significantly down-regulated after stimulation with CM-Silica given to the spheroids. In contrast, the anti-apoptotic protein Bcl-2 is significantly up-regulated. The trend of spheroids apoptotic proteins on days 1, 7, and 14 of the intervention is the same, with the same down-regulation trend, corresponding to the immunofluorescence results.

In combination, the data suggest that silica-stimulation prompts myofibroblasts in spheroids to exhibit significant apoptosis resistance properties.

3.5. Apoptosis resistance in 3D spheroids may be related to the Nrf2/Bax pathway

As an essential factor in causing apoptosis, oxidative stress also plays an important role in the initiation of silicosis fibrosis, and GO enrichment shows that the biological processes of spheroids oxidative stress were likewise significantly altered after administering a silica-stimulated macrophage supernatant, such as the altered cellular regulation regarding the oxidative stress response. An emerging hypothesis is that the emergence of the spheroids apoptosis resistance phenomenon may be correlated with changes in oxidative stress.

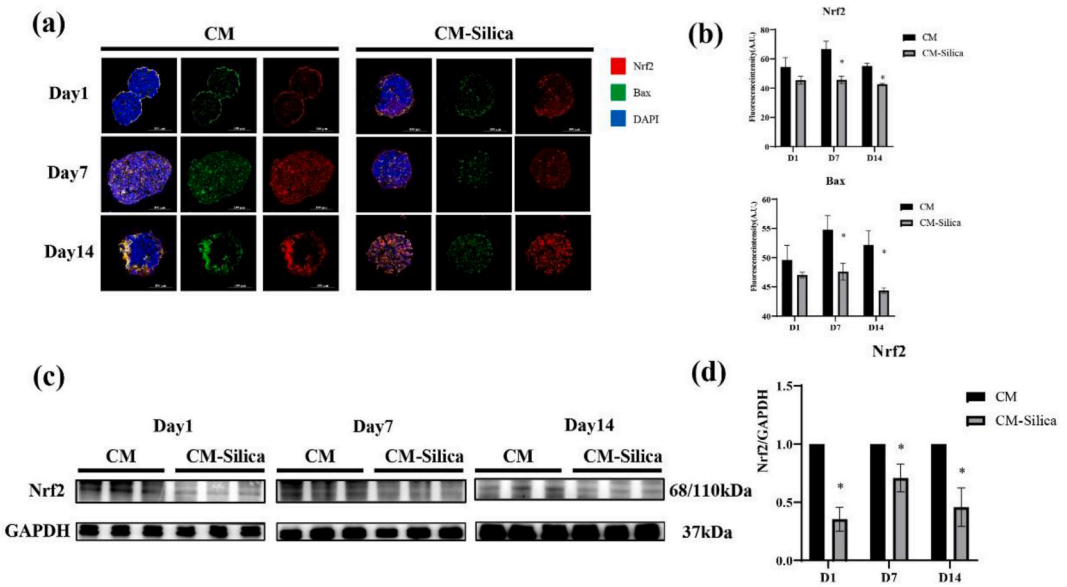

Fig. 5. (a) Immunofluorescence double staining results of model Nrf2, Bax proteins after 1, 7 and 14 days of stimulation of spheroids models by macrophage supernatant with/without silica-stimulation. (b) Results of statistical analysis of fluorescence intensity of Nrf2, Bax proteins, n = 3, *: $p < 0.05$. (c) Western blotting experiments of 3D model Nrf2 proteins after stimulation of spheroids models with/without silica-stimulated macrophage supernatant for 1, 7, and 14 days. (d) Results of statistical analysis of grey values, n = 3, *: $p < 0.05$ compared to CM. All data are expressed as mean ± SD.

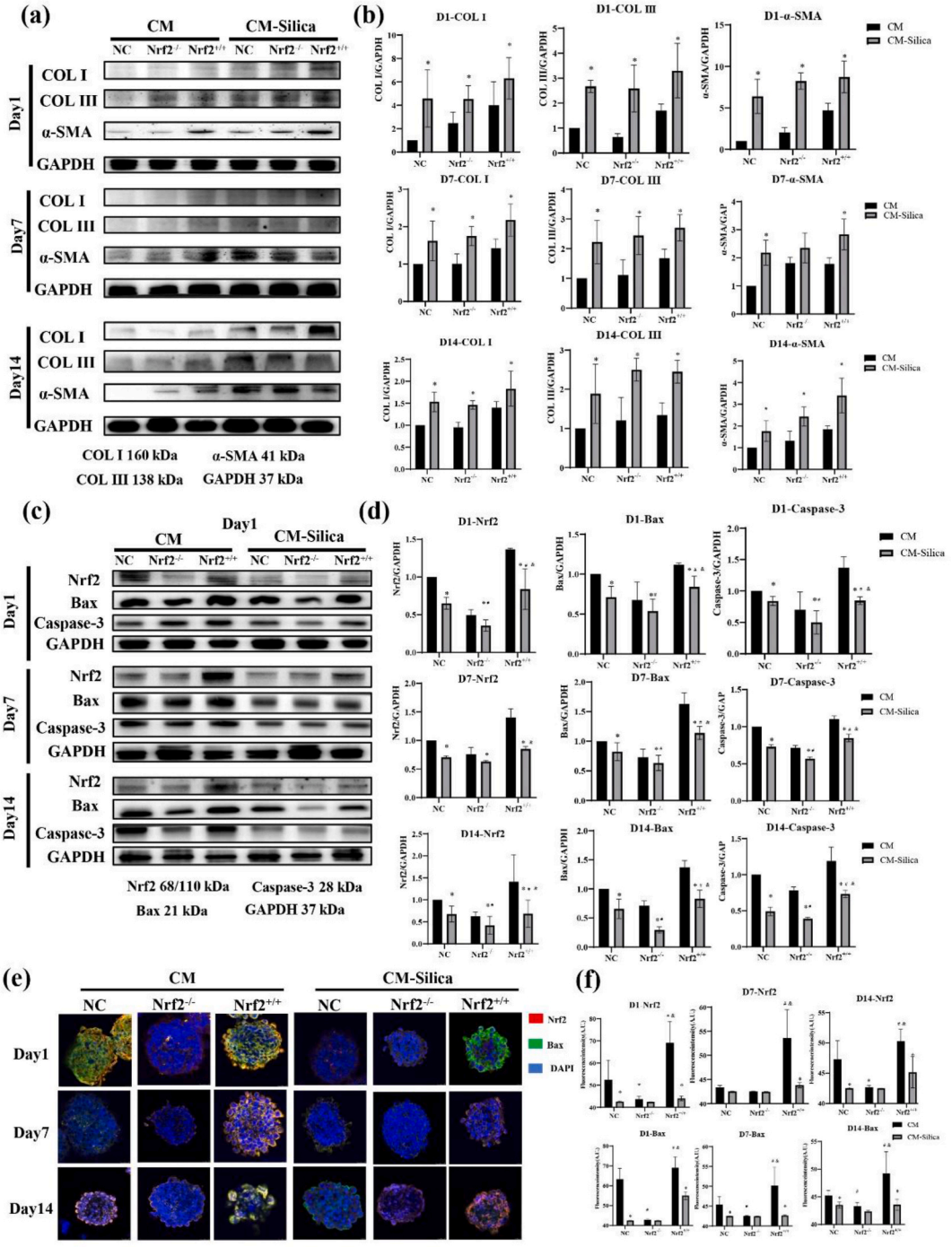

Fig. 6. (a) Results of Western Blot assay for fibrosis indexes (COL I, COL III, α-SMA) of spherocytes in NC, $Nrf2^{+/+}$ and $Nrf2^{-/-}$ groups after stimulation with/without silica-stimulated macrophage supernatants. (b) Results of statistical analysis of the grey value of fibrosis index assay, n = 3, *: $p < 0.05$ compared with NC group. (c) Results of Western Blot for Nrf2 and apoptosis-related indexes (Bax, Caspase-3) of spherical cells in the NC group, the $Nrf2^{+/+}$ group, and the $Nrf2^{-/-}$ group after stimulation with supernatants from macrophages with/without silica stimulation. (d) Results of statistical analysis of grey values, n = 3, *: $p < 0.05$ compared with CM (NC), #: $p < 0.05$ compared to CM ($Nrf2^{-/-}$); &: $p < 0.05$ compared to CM ($Nrf2^{+/+}$). (e) Results of Nrf2, Bax immunofluorescence of spherical cells in NC, $Nrf2^{+/+}$, and $Nrf2^{-/-}$ groups after stimulation of macrophage supernatants with/without silica stimulation. (f) Results of statistical analysis of fluorescence intensity, n = 3, *: $p < 0.05$ compared with the CM (NC), &: $p < 0.05$ compared to CM-Silica (NC).

Nrf2 is an important nuclear transcription factor in vivo, which is an essential indicator of oxidative stress, and its changed situation after silica stimulation is closely related to the fibrosis process. Therefore, variation of Nrf2 protein levels during the process of apoptosis resistance occurring in spheroids was analyzed to clarify the changes of oxidative stress and apoptosis caused by silica stimulation. Immunofluorescence staining of Nrf2 and Bax proteins on spheroids stained with silica stimulation for 1, 7, and 14 days was assessed. The results showed (Fig. 5(a)) that the expression sites of the two are very close to each other spatially, primarily concentrated in the peri spheroids area and also expressed in the centre of the spheroids. Nrf2 and Bax have a consistent down-regulation tendency after administration of different durations of silica stimulation.

Levels of the Nrf2 protein were quantified using Western Blot analysis, with Nrf2 levels decreasing significantly after administration of CM-Silica. Combined with the results of the Western Blot analysis of Bax protein, both protein levels changed in the same direction after the administration of silica stimulation. Such data infers that low expression of Nrf2 during silica-induced collagen deposition may be associated with low expression of Bax, which regulates apoptosis.

3.6. Apoptosis resistance in 3D spheroids acts through the Nrf2/Bax pathway

The Western blotting data concerning oxidative stress showed that the Nrf2 expression level is consistently lowest in the $Nrf2^{-/-}$ group and highest in the $Nrf2^{+/+}$ group in the CM group at different incubation times, demonstrating that a three-dimensional sphere model of Nrf2 silencing and overexpression was successfully developed. After silica stimulation, the Nrf2 levels in the spheroids of the NC, $Nrf2^{-/-}$, and $Nrf2^{+/+}$ groups were all significantly lower than those in the corresponding spheroids of the CM group. This outcome suggests that silica stimulation may lead to decreasing in the levels of anti-oxidative stress in myofibroblasts in spheroids (Fig. 6(a and b)).

Correspondingly, the expression of Bax and Caspase-3 demonstrates a clear consistency with the up/down regulation of Nrf2 (Fig. 6 (c and d)). In the CM group with different incubation times, Bax and Caspase-3 expression is significantly up-regulated with Nrf2 overexpression. In contrast, Bax and Caspase-3 expression was significantly down-regulated when Nrf2 is silenced, similar to the trend in the CM-Silica group. Additionally, silica stimulation results in a reduction of Bax and Caspase-3 in spheroids of the NC, $Nrf2^{-/-}$, and $Nrf2^{+/+}$ groups (compared to the three groups in the CM treatment). The expression trends of both metrics are consistently decreased whether stimulated for 1, 7, or 14 days. Immunofluorescence co-staining of Nrf2 and Bax shows the same expression trends as Western Blot (Fig. 6(e and f)).

To further verify the regulatory relationship between Nrf2 and Bax, the $Nrf2^{+/+}$ cell lines were exposed to Bax inhibitors and agonists. The results showed that the apoptosis indicators Bax and Caspase-3 are significantly down-regulated after using Bax inhibitors (Fig. 7(a and b)). Accordingly, Bax-induced apoptosis was on the rise after intervention with Bax agonists in the $Nrf2^{+/+}$ spheroid model (Fig. 7(c and d)). Finally, the expression of COL I in $Nrf2^{+/+}$ spheroids is significantly up-regulated following intervention with CM-silica (Fig. 6(a)). This phenomenon may be related to the role of Nrf2 in activating fibroblasts. Further studies are needed to investigate the possibility of tissue repair in the early stages of fibrosis.

4. Discussion

Silicosis is caused by prolonged exposure to silica, culminating in the development of pulmonary fibrosis. Numerous studies have explored the disease's onset mechanisms, yet there remains a deficiency in detailed in vitro models that can accurately simulate the progression of silicosis fibrosis. This study innovatively developed a 3D pulmonary spheroid model, utilising mouse lung-derived

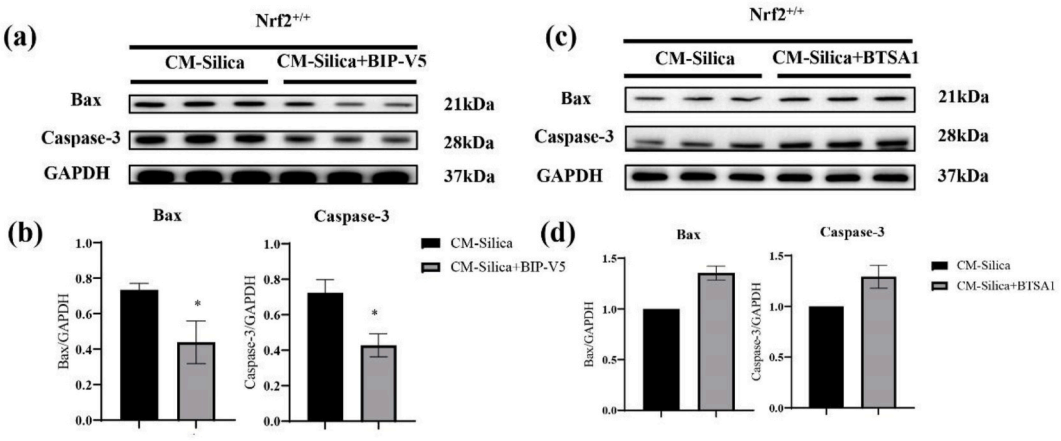

Fig. 7. (a) Apoptotic indexes of spheroids in the $Nrf2^{+/+}$ group after the intervention of Silica and Bax inhibitor (BIP–V5) was given to the spheroids. (b) Results of statistical analysis of grey values, n = 3, *: $p < 0.05$ compared with CM-Silica group. All data are expressed as mean ± SD. (c) Apoptotic indexes of spheroids in the $Nrf2^{+/+}$ group after the intervention of Silica and Bax agonist (BTSA1)were given to the spheroids. (d) Results of statistical analysis of grey values, n = 3, *: $p < 0.05$ compared with CM-Silica group. All data are expressed as mean ± SD.

decellularised matrices as scaffolds, coupled with self-assembled fibroblasts, to investigate the mechanisms underlying silicosis. Exposure to silica activates fibroblasts in the model, fostering a phenotype resistant to apoptosis through the Nrf2/Bax pathway. This new model has advanced the strategies of silicosis research by providing a unique approach and valuable insights into the mechanisms of myofibroblast apoptosis resistance in silicosis fibrosis, paving the way for potential therapeutic strategies.

In the realm of silicosis research, prioritising the development of fibroblast cellular models is essential due to their critical involvement in the disease's evolution. Presently, research predominantly utilises two-dimensional cell cultures, which are constrained by short cultivation periods, limiting the extent of cellular changes observed. Additionally, these models lack essential elements such as ECM support and a genuine in vivo microenvironment, restricting the comprehensive exhibition of cellular functionalities [19,20]. The current study successfully established a robust 3D spheroid model, integrating lung decellularised matrix from mouse and fibroblasts. This innovative model demonstrats an enhanced survival, persisting stably for at least fourteen days under silica-stimulated macrophage supernatant, outperforming the 2–3 days observed in conventional two-dimensional cultures. Unlike prevailing models reliant on collagen-based hydrogels [21–25], mouse lung-derived matrices, were incorporated recognizing the ECM's complexity and striving for a more accurate representation of diverse tissue ECM components [26,27]. This approach, grounded in biomimetic principles, fosters an environment conducive to authentic cell growth and functionality, overcoming limitations inherent in traditional two- and three-dimensional materials [28,29]. Silica exposure durations of 1, 7, and 14 days were chosen, as it is suggested that the 3D spheroids model could simulate the development of silicotic nodules very well. Consequently, to simulate the changes of silicotic nodules in the early stage, the developmental stage, and the fibrotic stage, incremental development at days 1, 7, and 14 were investigated to assess the changes occurring in myofibroblasts under the different time durations of the silica stimulation. Stimulated by silica, our model shows a marked progression of fibrosis characterised by increasing collagen fibres and a decrease in the number of cells in the interior, with the cells in the microspheres predominantly located on the outside or surface of the spheres. Consistent results for collagen volume and Western Blot analysis confirmed these data. Additionally, the ECM not only provides structural support but also significantly influences cell survival, growth, and apoptosis. This study has shown that the ECM components incorporated into our model, including Collagen I/III, fibronectin, and laminin, are crucial. Collagen I/III and fibronectin, primarily secreted by fibroblasts, serve not only as the principal structural and adhesive elements in tissue repair but also establish negative feedback mechanisms that are vital for maintaining tissue integrity and function [30]. These interactions between fibroblasts and the ECM components are pivotal in modulating cellular functions. Specifically, the engagement of fibroblasts with fibronectin through integrins and other surface receptors can activate signaling pathways such as PI3K/AKT, known to promote cell survival and confer resistance to apoptosis [31]. In this study, incorporating moderate levels of ECM components enhances fibroblast proliferation, highlighting its regulatory influence on cellular functions. These findings emphasise the ability of the newly developed model to realistically simulate the complex progression of silicosis nodules in silicosis, marking a fundamental advance in the field.

Silica stimulation triggers a complex immune response that significantly affects fibroblast behaviour, which is essential for understanding diseases such as silicosis. Upon exposure to silica, macrophages recognise silica particles as pathogen-associated molecular patterns, leading to their activation and subsequent secretion of pro-inflammatory cytokines like IL-1 and TNF [32,33]. These cytokines play a crucial role in the activation and proliferation of fibroblasts involved in the fibrotic processes seen in silicotic tissues. Research shows that silica exposure increases proliferative responses and cytokine secretion in peripheral blood mononuclear cells (PBMCs) from silicosis patients, indicating a specific modulation of the immune response compared to healthy controls [34]. This heightened response can lead to increased fibroblast activity and fibrosis, illustrating a direct link between immune cell stimulation by silica and fibroblast-mediated tissue remodeling. Understanding these intercellular interactions after silica stimulation offers insights into the pathogenic mechanisms driving fibrosis and potential autoimmune complications [35]. The current model used silica-stimulated macrophage supernatant as the microenvironment for the 3D spheroids to mimic the immune responses and cell interactions experienced by fibroblasts in vivo. Current research suggests that silica enters the organism and stimulates the production of a large number of cytokines, inflammatory factors, and reactive oxygen species (ROS), which ultimately leads to the creation of a predominantly inflammatory and oxidative stress environment in the lungs, marking the initial stage in the development of silicosis fibrosis [36]. The observed impairment of antioxidant functions in the lung tissues of affected individuals further substantiates this premise [37]. Nrf2 is a pivotal transcription factor in oxidative redox regulation, crucial for maintaining cellular homeostasis during oxidative stress by facilitating the protective expression of antioxidant genes [38]. Regarding pulmonary fibrosis, a reduced expression of Nrf2 has been observed within lesions [39], the significance of which remains ambiguous. Fibroblasts, transforming into myofibroblasts during oxidative stress, are instrumental in early tissue repair, synthesising essential extracellular matrix components for tissue regeneration [40,41]. After recovery, myofibroblasts can initiate their mitochondrial apoptosis pathway [42]. However, a notable "apoptosis paradox" is present during fibrosis, where myofibroblasts exhibit apoptosis resistance, unlike the susceptible epithelial cells, contributing significantly to the progression of silicosis fibrosis [43,44]. This resistance is potentially attributed to an imbalance among the Bcl-2 family proteins, emphasising a nuanced complexity in the molecular mechanisms underlying fibrotic processes [45]. The spheroid model simulating the progression of fibroblasts in fibrosis was utilised in this study to clarify the mechanism of apoptosis resistance in myofibroblasts during silicosis fibrosis. Upon exposure to silica-stimulated macrophage supernatants, a notable downregulation of apoptosis-related gene expression, Immunofluorescent staining and protein Western blotting of Bax/Bcl-2 proteins in myofibroblasts were observed, confirming the presence of an apoptosis-resistant phenotype instigated by silica stimulation. Additionally, the expression of Nrf2, an essential protein for oxidative stress, was significantly reduced. Combined with the results of transcriptome sequencing analysis, such data infers that oxidative stress plays an important role in the fibrogenic process, and that the differential genes were mainly enriched in the functions of "response to oxidative stress", "oxidative stress acting on NADPH", and so on, after the administration of silica stimulation. Wang [46] reports that Nrf2-mediated oxidative damage occurs mainly in fibroblasts by regulating endogenous glutathione metabolism through transcriptomic analysis of lung tissues from

silica-dusted mice, and that Nrf2-mediated oxidative damage occurs mainly in fibroblasts by regulating endogenous glutathione metabolism through the regulation of Nrf2-mediated oxidative damage and endogenous glutathione metabolic pathway to attenuate silica-induced oxidative stress and lung injury. Silica also induces impaired mitochondrial function, and Wu [47] reported that mitochondria were impaired in mouse lung tissue in a silica-induced pulmonary fibrosis model, and that this pathway may be an important feature in the pathogenesis of silica-induced pulmonary fibrosis. Unbiased analysis using quantitative mass spectrometry by Qu [48] revealed that proteins involved in mitochondrial metabolism showed specific up-regulation during the formation of myofibroblasts, which mainly includes glucose-6-phosphate dehydrogenase (G6PD) and isocitrate dehydrogenase 1 (IDH1), two enzymes essential for cell membrane NADPH generation that were significantly down-regulated. In contrast, mitochondrial folate supplementation alleviated oxidative stress and inhibits the differentiation of fibroblasts into myofibroblasts, suggesting that myofibroblasts can undergo mitochondrial oxidative stress induced by silica, and that this pathway plays a key role in activating the process of myofibroblasts, consistent with data from this current study. Moreover, there is a close spatial co-localisation between Nrf2 and the apoptosis-regulating protein Bax. This co-localisation suggests a potential interaction between oxidative stress and the anti-apoptotic capacity of myofibroblasts, thus implicating a critical role for Nrf2 depletion and the anti-apoptotic capacity of myofibroblasts in the development of silicosis fibrosis. These findings emphasise the importance of these molecular interactions in understanding and potentially mitigating silicosis pathogenesis.

An NFE2L2 gene silencing and overexpression in NIH/3T3 cells using lentiviral transfection was developed to elucidate the regulatory relationship between Nrf2 and Bax in the mechanism of myofibroblast apoptosis resistance during silicosis fibrosis, constructing identical 3D spheroid models for experimentation. The fibrosis model proved stable, consistent with prior findings regarding pre-lentiviral intervention. When silica stimulation was applied to $Nrf2^{+/+}$ spheroids, a notable upregulation of the apoptosis indicator Bax in myofibroblasts was observed, whereas $Nrf2^{-/-}$ spheroids showed the opposite effect. Such data infers a co-regulatory relationship between Nrf2 and Bax in influencing myofibroblast apoptosis resistance mechanisms. The apoptotic index of the spheroids showed a significant upregulation after administering Bax inhibitors and was investigated to further understand Nrf2-overexpressing spheroids after intervention with Bax inhibitors and agonists. In contrast, the apoptotic index of the spheroids showed a significant upregulation after the use of Bax agonists. Such data demonstrates phenotypically that the Nrf2/Bax pathway plays a role in myofibroblast apoptosis resistance. A comprehensive analysis of the results indicates that sustained silica stimulation leads to decreased Nrf2 expression in myofibroblasts, fostering an apoptosis-resistant phenotype mediated through the Nrf2/Bax pathway. Current research on oxidative stress and apoptosis in fibrosis is relatively advanced. Zhang [49] reports that activating the Nrf2/Keap-1 pathway effectively inhibits ROS production and suppresses the proliferation and migration of fibroblast-like synoviocytes in rheumatoid arthritis, leading to cell apoptosis via the mitochondrial pathway. However, the data in the current study uniquely demonstrates the mechanisms of myofibroblast apoptosis resistance in silicosis fibrosis.

In addition to the primary findings, an intriguing phenomenon was also observed. When the $Nrf2^{+/+}$ spheroids are exposed to silica-stimulated macrophage supernatant, there is a notable increase in the expression of fibrosis-related markers COL I. Such data infers that Nrf2 might play a pivotal role in the activation pathways of myofibroblasts, particularly during the early stages of tissue repair in silicosis fibrosis. Earlier research indicated that activating the transcription factor Nrf2 could counteract silicon dioxide-induced lung fibrosis in mice [13]. The current study builds on this investigation, further emphasising that persistent activation of Nrf2 in myofibroblasts may indeed offer a viable therapeutic approach against silicosis fibrosis.

In this study, a successful 3D lung spheroid model is established, employing fibroblasts and acellular lung matrices to investigate the apoptosis-resistant phenotype of myofibroblasts in silicosis fibrosis. The study elucidates the pathways that facilitate this resistance under silica stimulation, offering valuable theoretical insights for the future treatment strategies of silicosis fibrosis. Despite these advancements, the model—focused predominantly on fibroblasts—does not fully encapsulate the complexity of silicosis development. Recognizing these limitations, future research will be focussed towards constructing more holistic in vitro models and leveraging the 3D model to unearth novel therapeutic approaches for combating silicosis fibrosis.

5. Conclusion

In conclusion, the current study establishes a novel fibroblast culture model that adequately mimics the changes that occur in fibroblasts during development in silicosis. It is clearly demonstrated that silica increases collagen secretion and deposition in the model and promotes an apoptosis-resistant phenotype in myofibroblasts. This phenotype functions through the Nrf2/Bax pathway. The outcomes provide an excellent theoretical basis and research tools for exploring the pathogenesis of silicosis.

Ethical approval

The Capital Medical University of Laboratory Animal Care and Use Committee approved this study (AEEI-2022–242). All efforts were made to minimize the suffering of the animals.

Consent to publish

Not applicable.

Data availability statement

Data relevant to this study are presented in the manuscript or supplementary material. And the datasets used and/or analyzed during the current study are available from the corresponding author on reasonable request.

CRediT authorship contribution statement

Wenming Xue: Writing – review & editing, Writing – original draft, Data curation, Conceptualization. **Jiaxin Wang:** Writing – review & editing, Validation. **Yao Hou:** Methodology. **Di Wu:** Investigation. **Hongwei Wang:** Validation. **Qiyue Jia:** Data curation. **Qiyue Jiang:** Methodology. **Yan Wang:** Methodology, Investigation. **Chenzhao Song:** Methodology. **Yifei Wang:** Methodology. **Zhonghui Zhu:** Methodology, Investigation. **Lin Tian:** Writing – review & editing, Writing – original draft, Methodology, Investigation.

Declaration of competing interest

The authors declare the following financial interests/personal relationships which may be considered as potential competing interests:Tian lin reports financial support was provided by National Natural Science Foundation of China. If there are other authors, they declare that they have no known competing financial interests or personal relationships that could have appeared to influence the work reported in this paper.

Acknowledgment and funding sources

This study was supported by the National Natural Science Foundation of China. (No. 81973008, 81602832, 81872595).

Appendix A. Supplementary data

Supplementary data to this article can be found online at https://doi.org/10.1016/j.heliyon.2024.e33585.

References

[1] S. Tan, S. Chen, The mechanism and effect of autophagy, apoptosis, and pyroptosis on the progression of silicosis, Int. J. Mol. Sci. 22 (15) (2021) 8110.
[2] H. Barnes, N.S.L. Goh, T.L. Leong, R. Hoy, Silica-associated lung disease: an old-world exposure in modern industries, Respirology 24 (12) (2019) 1165–1175.
[3] The Lancet Respiratory M, The world is failing on silicosis, Lancet Respir. Med. 7 (4) (2019) 283.
[4] V.J. Thannickal, G.B. Toews, E.S. White, Iii JP. Lynch, F.J. Martinez, Mechanisms of pulmonary fibrosis, Annu. Rev. Med. 55 (1) (2004) 395–417.
[5] M. Zhao, L. Wang, M. Wang, S. Zhou, Y. Lu, H. Cui, et al., Targeting fibrosis: mechanisms and clinical trials, Signal Transduct. Targeted Ther. 7 (1) (2022) 206.
[6] A. Desmouliere, I.A. Darby, B. Laverdet, F. Bonté, Fibroblasts and myofibroblasts in wound healing, Clin. Cosmet. Invest. Dermatol. 7 (2014) 301–311.
[7] S. Mukundan, P. Singh, A. Shah, R. Kumar, K.C. O'Neill, C.L. Carter, et al., In vitro miniaturized tuberculosis spheroid model, Biomedicines 9 (9) (2021) 1209.
[8] J. Nardi, S. Nascimento, G. Göethel, B. Gauer, E. Sauer, N. Fão, et al., Inflammatory and oxidative stress parameters as potential early biomarkers for silicosis, Clin. Chim. Acta 484 (2018) 305–313.
[9] X. Dang, B. He, Q. Ning, Y. Liu, J. Guo, G. Niu, et al., Alantolactone suppresses inflammation, apoptosis and oxidative stress in cigarette smoke-induced human bronchial epithelial cells through activation of Nrf2/HO-1 and inhibition of the NF-κB pathways, Respir. Res. 21 (1) (2020).
[10] M.F. Acosta, P. Muralidharan, C.L. Grijalva, M.D. Abrahamson, D. Hayes, J.R. Fineman, et al., Advanced therapeutic inhalation aerosols of a Nrf2 activator and RhoA/Rho kinase (ROCK) inhibitor for targeted pulmonary drug delivery in pulmonary hypertension: design, characterization, aerosolization, in vitro 2D/3D human lung cell cultures, and in vivo efficacy, Ther. Adv. Respir. Dis. (15) (2021), 1753466621998245.
[11] M. Tang, Z. Yang, J. Liu, X. Zhang, L. Guan, X. Liu, et al., Combined intervention with N-acetylcysteine and desipramine alleviated silicosis development by regulating the Nrf2/HO-1 and ASMase/ceramide signaling pathways, Ecotoxicol. Environ. Saf. 242 (2022) 113914.
[12] L. Hecker, N.J. Logsdon, D. Kurundkar, A. Kurundkar, K. Bernard, T. Hock, et al., Reversal of persistent fibrosis in aging by targeting Nox4-Nrf2 redox imbalance, Sci. Transl. Med. 6 (231) (2014).
[13] Z. Zhu, Q. Li, C. Xu, J. Zhao, S. Li, Y. Wang, et al., Sodium tanshinone IIA sulfonate attenuates silica-induced pulmonary fibrosis in rats via activation of the Nrf2 and thioredoxin system, Environ. Toxicol. Pharmacol. 80 (2020).
[14] A. Wu, B. Feng, J. Yu, L. Yan, L. Che, Y. Zhuo, et al., Fibroblast growth factor 21 attenuates iron overload-induced liver injury and fibrosis by inhibiting ferroptosis, Redox Biol. 46 (2021).
[15] B. Hinz, S.H. Phan, V.J. Thannickal, A. Galli, M.-L. Bochaton-Piallat, G. Gabbiani, The myofibroblast, Am. J. Pathol. 170 (6) (2007) 1807–1816.
[16] J.C. Horowitz, I.O. Ajayi, P. Kulasekaran, D.S. Rogers, J.B. White, S.K. Townsend, et al., Survivin expression induced by endothelin-1 promotes myofibroblast resistance to apoptosis, Int. J. Biochem. Cell Biol. 44 (1) (2012) 158–169.
[17] K. McElhinney, M. Irnaten, C. O'Brien, p53 and myofibroblast apoptosis in organ fibrosis, Int. J. Mol. Sci. (7) (2024) 6737.
[18] N.J.L. Kosuke Kato, Yoon-Joo Shin, Sunny Palumbo, Knox Adam, Joseph D. Irish, Skye P. Rounseville, Sydney R. Rummel, Mohamed Mohamed, Kareem Ahmad, Johnny M. Trinh, Deepali Kurundkar, Kenneth S. Knox, Victor J. Thannickal, Louise Hecker, Impaired myofibroblast Dedifferentiation contributes to nonresolving fibrosis in aging, Am. J. Respir. Cell Mol. Biol. 62 (5) (2020) 633–644.
[19] A.I. Vazquez-Armendariz, M.M. Barroso, E. El Agha, S. Herold, 3D in vitro models: novel insights into idiopathic pulmonary fibrosis pathophysiology and drug screening, Cells 11 (9) (2022) 1526.
[20] M. Štampar, B. Breznik, M. Filipič, B. Žegura, Characterization of in vitro 3D cell model developed from human hepatocellular carcinoma (HepG2) cell line, Cells 9 (12) (2020).
[21] M. Tekguc, R.C.V. Gaal, S.G.M. Uzel, N. Gupta, L.V. Riella, J.A. Lewis, et al., Kidney organoids: a pioneering model for kidney diseases, Transl. Res. 250 (2022) 1–17.
[22] E. Mohr, T. Thum, C. Bär, Accelerating cardiovascular research: recent advances in translational 2D and 3D heart models, Eur. J. Heart Fail. 24 (10) (2022) 1778–1791.

[23] P. Mukhopadhyay, V. Prestigiacomo, A. Weston, S. Messner, F. Lampart, L. Suter-Dick, Pro-fibrotic compounds induce stellate cell activation, ECM-remodelling and Nrf2 activation in a human 3D-multicellular model of liver fibrosis, PLoS One 12 (6) (2017).
[24] W. Shin, H.J. Kim, 3D in vitro morphogenesis of human intestinal epithelium in a gut-on-a-chip or a hybrid chip with a cell culture insert, Nat. Protoc. 17 (3) (2022) 910–939.
[25] A. Mariappan, G. Goranci-Buzhala, L. Ricci-Vitiani, R. Pallini, J. Gopalakrishnan, Trends and challenges in modeling glioma using 3D human brain organoids, Cell Death Differ. 28 (1) (2020) 15–23.
[26] X. Zhang, X. Chen, H. Hong, R. Hu, J. Liu, C. Liu, Decellularized extracellular matrix scaffolds: recent trends and emerging strategies in tissue engineering, Bioact. Mater. 10 (2022) 15–31.
[27] M.E. Smithmyer, L.A. Sawicki, A.M. Kloxin, Hydrogel scaffolds asin vitromodels to study fibroblast activation in wound healing and disease, Biomater. Sci. 2 (5) (2014) 634–650.
[28] B. Mahendiran, S. Muthusamy, R. Selvakumar, N. Rajeswaran, S. Sampath, S.N. Jaisankar, et al., Decellularized natural 3D cellulose scaffold derived from Borassus flabellifer (Linn.) as extracellular matrix for tissue engineering applications, Carbohydr. Polym. 272 (2021).
[29] B. Wang, T. Qinglai, Q. Yang, M. Li, S. Zeng, X. Yang, et al., Functional acellular matrix for tissue repair, Mater. Today Bio (18) (2022) 100530.
[30] M.A. Karsdal, S.H. Nielsen, D.J. Leeming, L.L. Langholm, M.J. Nielsen, T. Manon-Jensen, A. Siebuhr, N.S. Gudmann, S. Rønnow, J.M. Sand, S.J. Daniels, J. H. Mortensen, D. Schuppan, The good and the bad collagens of fibrosis - their role in signaling and organ function, Adv. Drug Deliv. Rev. 121 (2017 Nov 1) 43–56.
[31] J. Ji, L. Chen, Y. Zhuang, Y. Han, W. Tang, F. Xia, Fibronectin 1 inhibits the apoptosis of human trophoblasts by activating the PI3K/Akt signaling pathway, Int. J. Mol. Med. 46 (5) (2020 Nov) 1908–1922.
[32] B. Pernis, Silica and the immune system, Acta Biomed. 76 (Suppl 2) (2005) 38–44.
[33] K.M. Pollard, Silica, silicosis, and autoimmunity, Front. Immunol. 7 (2016 Mar 11) 97.
[34] K. Peukert, F. Steinhagen, M. Fox, C. Feuerborn, S. Schulz, B. Seeliger, P. Schuss, M. Schneider, S. Frede, A. Sauer, C. Putensen, E. Latz, C. Wilhelm, C. Bode, Tetracycline ameliorates silica-induced pulmonary inflammation and fibrosis via inhibition of caspase-1, Respir. Res. 23 (1) (2022 Feb 7) 21.
[35] X. Guo, C. Jagannath, M.G. Espitia, X. Zhou, Uptake of silica and carbon nanotubes by human macrophages/monocytes induces activation of fibroblasts in vitro – potential implication for pathogenesis of inflammation and fibrotic diseases, Int. J. Immunopathol. Pharmacol. 25 (3) (2012 Jul-Sep) 713–719.
[36] Y. Zhao, G. Xu, H. Li, M. Chang, C. Xiong, Y. Tao, et al., Genome-wide mRNA profiling identifies the NRF2-regulated lymphocyte oxidative stress status in patients with silicosis, J. Occup. Med. Toxicol. 16 (1) (2021) 40.
[37] P.A. Reyfman, J.M. Walter, N. Joshi, K.R. Anekalla, A.C. McQuattie-Pimentel, S. Chiu, et al., Single-cell transcriptomic analysis of human lung provides insights into the pathobiology of pulmonary fibrosis, Am. J. Respir. Crit. Care Med. 199 (12) (2019) 1517–1536.
[38] T. Sekine, T. Hirata, S. Ishikawa, S. Ito, K. Ishimori, K. Matsumura, et al., Regulation of NRF2, AP-1 and NF-κB by cigarette smoke exposure in three-dimensional human bronchial epithelial cells, J. Appl. Toxicol. 39 (5) (2018) 717–725.
[39] Y. Wang, J. Wei, H. Deng, L. Zheng, H. Yang, X. Lv, The role of Nrf2 in pulmonary fibrosis: molecular mechanisms and treatment approaches, Antioxidants 11 (9) (2022).
[40] C. Hung, G. Linn, Y.-H. Chow, A. Kobayashi, K. Mittelsteadt, W.A. Altemeier, et al., Role of lung pericytes and resident fibroblasts in the pathogenesis of pulmonary fibrosis, Am. J. Respir. Crit. Care Med. 188 (7) (2013) 820–830.
[41] D. Chanda, E. Otoupalova, S.R. Smith, T. Volckaert, S.P. De Langhe, V.J. Thannickal, Developmental pathways in the pathogenesis of lung fibrosis, Mol. Aspect. Med. 65 (2019) 56–69.
[42] F. Migneault, M.-J. Hébert, Autophagy, tissue repair, and fibrosis: a delicate balance, Matrix Biol. 100–101 (2021) 182–196.
[43] X.X. Tang, Q.Y. Yu, Irreversibility of pulmonary fibrosis, Aging and disease 13 (1) (2022).
[44] J.L. Larson-Casey, J.S. Deshane, A.J. Ryan, V.J. Thannickal, A.B. Carter, Macrophage Akt1 kinase-mediated mitophagy modulates apoptosis resistance and pulmonary fibrosis, Immunity 44 (3) (2016) 582–596.
[45] R. Singh, A. Letai, K. Sarosiek, Regulation of apoptosis in health and disease: the balancing act of BCL-2 family proteins, Nat. Rev. Mol. Cell Biol. 20 (3) (2019) 175–193.
[46] L. Wang, M. Zhao, R. Qian, M. Wang, Q. Bao, X. Chen, W. Du, L. Zhang, T. Ye, Y. Xie, B. Zhang, L. Peng, Y. Yao, Nicotinamide mononucleotide ameliorates silica-induced lung injury through the nrf2-regulated glutathione metabolism pathway in mice, Nutrients 15 (1) (2022 Dec 28) 143.
[47] Q. Wu, T. Xu, Y. Liu, Y. Li, J. Yuan, W. Yao, Q. Xu, W. Yan, C. Ni, miR-1224-5p mediates mitochondrial damage to affect silica-induced pulmonary fibrosis by targeting BECN1, Int. J. Mol. Sci. 18 (11) (2017 Nov 7) 2357.
[48] Y. Qu, R. Zhai, D. Wang, Z. Wang, G. Hou, C. Wu, M. Tang, X. Xiao, J. Jiao, Y. Ba, F. Zhou, J. Qiu, W. Yao, Mitochondrial folate pathway regulates myofibroblast differentiation and silica-induced pulmonary fibrosis, J. Transl. Med. 21 (1) (2023 Jun 6) 365.
[49] Y. Zhang, G. Wang, T. Wang, W. Cao, L. Zhang, X. Chen, Nrf2–Keap1 pathway–mediated effects of resveratrol on oxidative stress and apoptosis in hydrogen peroxide–treated rheumatoid arthritis fibroblast-like synoviocytes, Ann. N. Y. Acad. Sci. 1457 (1) (2019) 166–178.